Maskless laser tailoring of conical pillar arrays for antireflective biomimetic surfaces

Lei Wang,[1] Bin-Bin Xu,[1] Qi-Dai Chen,[1,3] Zhuo-Chen Ma,[1] Ran Zhang,[1] Qing-Xue Liu,[1] and Hong-Bo Sun[1,2,4]

[1]*State Key Laboratory on Integrated Optoelectronics, College of Electronic Science and Engineering, Jilin University, 2699 Qianjin Street, Changchun 130012, China*

[2]*College of Physics, Jilin University, 119 Jiefang Road, Changchun 130023, China*

[3]*e-mail: chenqd@jlu.edu.cn*

[4]*e-mail: hbsun@jlu.edu.cn*

**Corresponding author: hbsun@jlu.edu.cn*

Received July 1, 2011; revised July 31, 2011; accepted July 31, 2011;
posted August 1, 2011 (Doc. ID 150192); published August 17, 2011

Herein, we report a facile approach for rapid and maskless production of subwavelength structured antireflective surfaces with high and broadband transmittance—direct laser interference ablation. The interfered laser beams were introduced into the surface of a bare optical substrate, where structured surfaces consisting of a micropillar array were produced by two-step laser irradiation in the time frame of seconds. A multiple exposure of the two-beam interference approach was proposed instead of multiple-beam interference to simply realize planar patterns of a high aspect ratio. Tall sinusoidal pillars were created and shaped by pulse shot number control. As an example of the application, zinc sulfide substrates were processed with the technology, from which high transmission at an infrared wavelength, over 92%, at normal incidence was experimentally achieved. © 2011 Optical Society of America

OCIS codes: 050.0050, 090.0090, 220.0220, 240.0240.

High transmittance is essential to window materials widely used in optical detection, solar cells, organic light-emitting diodes, and high-power laser systems [1]. To gain high transmittance, multilayer films are coated to optical substrates for antireflection. However, the films often suffer from ease of shedding or cracking due to mechanical scratching and deforming from thermal expansion or low-temperature shrinkage. Inspired by moth eyes, microstructured surfaces were developed as an alternative solution [2–4]. The surface consists of pillars of intervals smaller than the propagating wavelength. It is the subwavelength structures that provide an effective refractive-index gradient between air and the substrate. They effectively suppress the Fresnel reflection and improve the transmission of light through the interface [4–7].

Approaches such as *e*-beam lithography [7], dry etching lithography [8,9], photoetching lithography [10,11], nanoimprint lithography [12], and laser ablation by mask-dragging [13] have been successfully developed to fabricate two-dimensional (2D) antireflective surfaces (ARSs). Generally, these fabrication procedures consist of two typical steps: (i) lithography patterning of sacrificial layer, e.g., exposed photoresist [7–11,14–16], self-assembled colloidal crystals [17], the reunion spheres of melted metal films and self-assembled monolayer islands [18,19], and (ii) subsequent etching of target substrates, e.g., *e*-beam etching, reactive ion etching, and inductively coupled plasma etching under the protection of the sacrifice layers. These works have not only proved the concept validity of ARSs for conformable optics, but also offered deep insight into ARS physics. However, these methods are generally limited to particular substrate species. Particularly for hard-processing window materials, such as sapphire and zinc sulfide, the etching processes pose serious problems of resist durability and low efficiency of material removal. So a micronanopatterning technology applicable to various substrate materials is desired.

We report a facile approach for rapid and maskless production of subwavelength structured surfaces with high and broadband transmittance, that is, direct laser interference ablation (D-LIA). The interfered lasers were not utilized for creation of sacrificial patterns as generally did [20], but it was introduced into the surface of bare optical substrates, where structured surfaces consisting of micropillar arrays were produced by a double-step laser irradiation in time frame of seconds. No mask preparation and pattern transfer procedures are needed any more. A multiple exposure of two-beam interference ablation (TBIA) approach was proposed instead of multiple-beam interference to simply realize planar patterns of high aspect ratio. Well-sharpened pillars were attained by pulse shots number control, which provides an effective index gradient for high and broadband transmittance in various optical substrates.

A schematic of multiple exposure of TBIA is presented in Fig. 1(a). A frequency-tripled, *Q*-switched, single-mode Nd:YAG laser (Spectra-Physics) with the emission wavelength of 355 nm, frequency of 10 Hz, and pulse duration

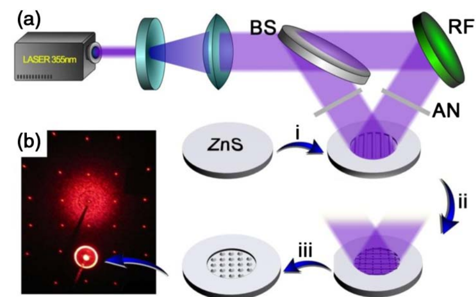

Fig. 1. (Color online) (a) Schematic of multiple exposure of TBIA: BS, beam splitter; RF, reflector; AN, attenuation mirror. (b) Projection of diffraction spots of the micropillar array that was actually created by the TBIA.

0146-9592/11/173305-03$15.00/0 © 2011 Optical Society of America

of 10 ns was employed for the experiment. In the initial step, one-dimensional gratings were obtained by TBIA. Materials at the light intensity maxima sites were more heavily ablated and removed than at the dark sites in the durative interference waves. The periods of the grating could be designed by changing the angle between the two laser beams, ϕ, according to

$$\Lambda = \frac{\lambda_F}{2\sin(\phi/2)}, \tag{1}$$

where λ_F is the laser wavelength of fabrication. In the following steps, the substrate was rotated by a certain angle along the surface normal of the substrate according to desired patterns. Taking square micropillar arrays as an example, a second TBIA was carried out in the perpendicular direction, i.e., a substrate rotation angle of 90°. The diameter of the round area of the uniform pillar arrangement is around 1 cm under single-shot exposures. Judging from the projection of diffraction spots of the micropillar array that was actually created by the TBIA [Fig. 1(b)], the structure should be well defined and is of high optical quality. This is confirmed by the scanning electron microscopic (SEM) images in Fig. 2.

In the current research, we take infrared window material of zinc sulfide (ZnS) as an example, and correspondingly, a 355 nm wavelength ultraviolet laser was chosen due to the good linear optical absorption in Fig. 2(a) measured by a Shimadzu UV-3600 spectrometer equipped with an integrating sphere detector. The grating in Fig. 2(b) shows a period of $\Lambda = 1\,\mu$m under $\phi = 20.45°$. By double exposure of TBIA, arrays of varied micropillar intervals of $\Lambda = 2\,\mu$m [Fig. 2(d)], $3\,\mu$m [Fig. 2(e)], and $4\,\mu$m [Fig. 2(f)] resulted from $\phi = 10.18°$, 6.78°, 5.09°, respectively, which are in good accordance with those predicted by Eq. (1). The exposure pulses are (14,7), (22,14), (30,18), and (40,24) from Figs. 2(c)–2(f), respectively, under single-pulse energy of 110 mJ.

The planar periodicity is important to guarantee homogeneous transmission at different sites of windows, but it is not a perquisite for antireflection. The pillar height and shape (sharpness) determine the transmission rate of an ARS [5,6,21]. The approximate theoretical minimum thickness of the structured layer, i.e., the pillar height reaching 100% transmittance, is determined by the following formula [5]:

$$h_{\min} = \frac{\lambda_P}{4\sqrt{n_1 n_2}}, \tag{2}$$

where λ_p is the propagating wavelength and n_1 and n_2 are the refractive index of air and the optical substrate, respectively. Given $n_2 = 2.2$ for ZnS at a typical infrared wavelength of $\lambda_p = 10\,\mu$m, we have $h_{\min} = 1.67\,\mu$m. The actual ARS height of period of $3\,\mu$m achieved experimentally is more than $h_{\min}$ [Fig. 3(d)], which was achieved by approximately (30, 18, 18) shots of pulses under single-pulse energy of 110 mJ. The enhanced absorption at 355 nm in the grating region [Fig. 2(a)] promotes the process of the subsequent micropillar fabrication. In the first ablation, 30 pulse shots were needed to structure the gratings of 2.57 um in height, whereas 18 pulse shots were enough in the second ablation process to get the same height. It is expected that the pillar height increases versus the pulse shot numbers, but a saturation height is observed [21]. There is almost no absolute zero intensity region, and accumulation of the pulse shots leads to material removal at the pillar sites. The maximal pillar height is reached at the velocity balance of the pillar top cutting and their interval digging.

The above affect is able to be utilized to tailor the shape of the pillars, which determines the effective refractive-index profile thorough the structured layer. Calculation on reflection from a gradient refractive-index film indicates that sinusoidal and paraboloidal pillars are among the most efficient antireflection geometries [11,22]. The electric field component (Ex) distribution simulations of the interference field in the region of the gratings were implemented by the finite-difference time-domain (FDTD) method. Obviously, the light intensity is stronger in the right angle of the structures, which looks like crescents densely packed around the structures, and could accelerate the speed of sharpening the gratings and micropillars. So the gratings and pillars presented a curved top but not a rigorous step profile.

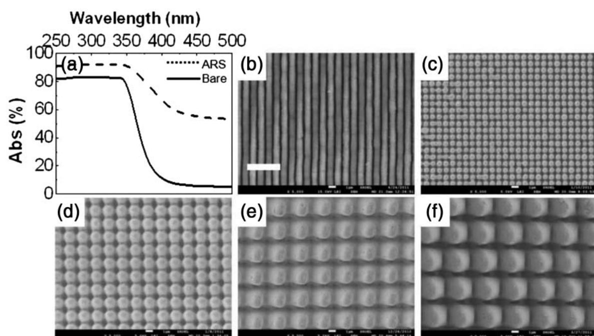

Fig. 2. (a) Absorption of ZnS ranging from 200 to 500 nm. The solid curve represents absorption of bare ZnS, while the dashed curve represents ZnS with the grating surface. (b) Gratings of period of $1\,\mu$m. Periodic square arrangement pillars of (c) 1, (d) 2, (e) 3, and (f) $4\,\mu$m. The scale bar for (b)–(f) represents $5\,\mu$m.

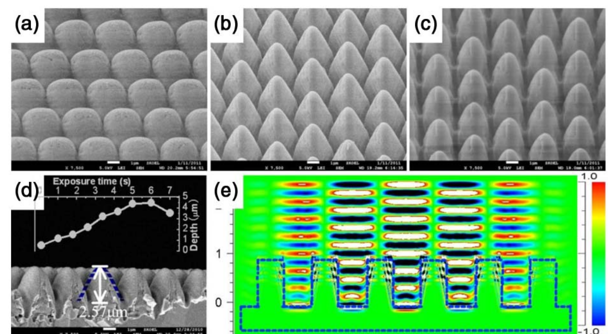

Fig. 3. (Color online) (a)–(c) SEM images of different depth and morphologies of micropillars by three times exposure of TBIA. (d) Cross-sectional image of hexagonal arrangement arrays with the depth of $2.57\,\mu$m. Inset, depth increase with exposure time (10 pulse shots per second). (e) Simulation of exchanges with interaction between gratings and two 355 nm interference beams by the FDTD method. The blue dashed profile represents the initial gratings formed by D-LIA. The scale bar represents $5\,\mu$m each.

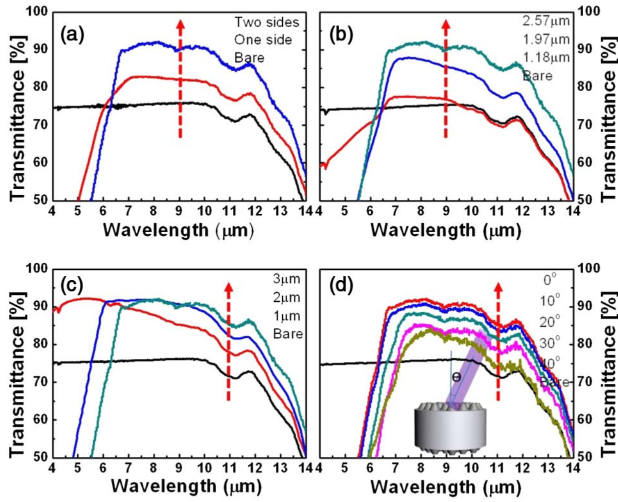

Fig. 4. (Color online) (a) Transmittance of single- and double-sided ARSs-ZnS. (b) Transmittance of double-sided ARSs-ZnS with different pillar depth. (c) Transmittance of double-sided ARSs-ZnS with different period. (d) Transmittance of double-sided ARSs-ZnS with incident angles ranging from 0° to 40°.

Experimentally, the pillar shaping was accomplished by manipulation of shot numbers of ablation. At the beginning of D-LIA (22, 14, 14) shots under laser pulse energy $E = 110\,\mathrm{mJ}$, the pillars appear as top-rounded rods [Fig. 3(a)]. The shoulders of the rods were gradually cut thinner (30, 16, 16) shots [Fig. 3(b)], resulting ultimately in a paraboloidal shape (30, 18, 18) shots [Fig. 3(c)]. Fitting the projective side profile of the pillars, one finds a good accordance with the sinusoidal function [Fig. 3(d)].

The optical properties of the ARSs-ZnS were characterized with Fourier transform infrared spectrometry (FT-IR, Nicolet 6700). Because Fresnel reflection occurs at the two surfaces of a window, a double-side structured surface was fabricated, which offers the best transmittance of 92.2% at $\lambda_p = 8.2\,\mu\mathrm{m}$ from normal incidence [Fig. 4(a)]. Transmittance of ZnS with double-sided ARS against the depth was measured [Fig. 4(b)]. For structures of $\Lambda = 1, 2$, and $3\,\mu\mathrm{m}$, the wave bands of transmittance exceeding 90% are located at 4.32–6.85 μm, 6.99–8.84 μm, and 8.92–10.15 μm [Fig. 4(c)], respectively. The antireflection wave bands are readily adjusted by the structure period, and therefore by selection of the interference beam angle, ϕ, and the attained high transmission makes the D-LIA-created ARSs practically useful. Incident-angle-dependent transmission is another important parameter to investigate. The bandwidth of transmittance over 80% maintains from 7.4 to 10.2 μm, even for $\theta = 40°$ [Fig. 4(d)], which is very difficult to achieve in conventional multilayer systems for the infrared wave bands. ARSs tested, except in Fig. 4(c), were of the period of 3 μm, and the structure height in Figs. 4(a) and 4(d) was 2.57 μm, shown in Fig. 3(d).

In conclusion, we report here a simple and rapid, one-step approach for fabricating antireflection structures on substrates consisting of various materials. The technology features direct ablating substrates with two interference beams without need of any mask. Varied transmission wave bands were fulfilled by adjusting the incident angle of the laser beams used for fabrication. Tall sinusoidal pillars were created and shaped by pulse shot number control. As an example of application, zinc sulfide substrates were processed with the technology, from which high transmission at infrared wavelength, over 92%, at normal incidence was experimentally achieved.

The authors gratefully acknowledge support from the National Natural Science Foundation of China (NSFC) (grants 61008035 and 90923037) and the 873 Program (grant 2009AA03Z401).

References

1. H. A. Macleod, *Thin-Film Optical Filters* (CRC Press, 2010).
2. P. B. Clapham and M. C. Hutley, Nature **244**, 281 (1973).
3. M. Ibn-Elhaj and M. Schadt, Nature **410**, 796 (2001).
4. J.-Q. Xi, M. F. Schubert, J. K. Kim, E. F. Schubert, M. Chen, S.-Y. Lin, W. Liu, and J. A. Smart, Nat. Photon. **1**, 176 (2007).
5. D. H. Raguin and G. M. Morris, Appl. Opt. **32**, 1154 (1993).
6. Y. M. Song and Y. T. Lee, Opt. Quantum Electron. **41**, 771 (2010).
7. M. Karlsson and F. Nikolajeff, Opt. Express **11**, 502 (2003).
8. C. Aydina, A. Zaslavsky, G. J. Sonek, and J. Goldstein, Appl. Phys. Lett. **80**, 2242 (2002).
9. Y.-J. Hung, S.-L. Lee, and L. A. Coldren, Opt. Express **18**, 6841 (2010).
10. J. Park, S. Yoon, K. Kang, and S. Jeon, Small **6**, 1981 (2010).
11. D. S. Hobbs and B. D. MacLeod, Proc. SPIE **5786**, 349 (2005).
12. Q. Chen, G. Hubbard, P. A. Shields, C. Liu, D. W. E. Allsopp, W. N. Wang, and S. Abbott, Appl. Phys. Lett. **94**, 263118 (2009).
13. M. Gower, Proc. SPIE **4559**, 53 (2001).
14. D. Wu, S.-Z. Wu, Q.-D. Chen, Y.-L. Zhang, J. Yao, X. Yao, L.-G. Niu, J. N. Wang, L. Jiang, and H.-B. Sun, Adv. Mater. **23**, 545 (2011).
15. A. Gombert, K. Rose, A. Heinzel, W. Horbelt, C. Zanke, B. Bläsi, V. Wittwer, Sol. Energy Mater. Sol. Cells **54**, 333 (1998).
16. D. Wu, Q.-D. Chen, H. Xia, J. Jiao, B.-B. Xu, X.-F. Lin, Y. Xu, and H.-B. Sun, Soft Matter **6**, 263 (2010).
17. Y. Li, J. Zhang, and B. Yang, Nano Today **5**, 117 (2010).
18. W.-T. Wang, N. Lu, J.-Y. Hao, H.-B. Xu, D.-P. Qi, and L.-F. Chi, J. Phys. Chem. C **114**, 1989 (2010).
19. J. W. Leem, J. S. Yu, Y. M. Song, and Y. T. Lee, Sol. Energy Mater. Sol. Cells **95**, 669 (2011).
20. N. D. Lai, W.-P. Liang, J.-H. Lin, C.-C. Hsu, and C.-H. Lin, Opt. Express **13**, 9605 (2005).
21. D. Yuan, R. Guo, Y. Wei, W. Wu, Y. Ding, Z. L. Wang, and S. Das, Adv. Funct. Mater. **20**, 3484 (2010).
22. Y. M. Song, H. J. Choi, J. S. Yu, and Y. T. Lee, Opt. Express **18**, 13063 (2010).